Perovskites Hot Paper

How to cite: *Angew. Chem. Int. Ed.* **2022,** *61,* e202115852
International Edition: doi.org/10.1002/anie.202115852
German Edition: doi.org/10.1002/ange.202115852

Interfacial Manganese-Doping in $CsPbBr_3$ Nanoplatelets by Employing a Molecular Shuttle

Linzhong Wu[+], Yiou Wang[+], Mariam Kurashvili, Amrita Dey, Muhan Cao, Markus Döblinger, Qiao Zhang, Jochen Feldmann, He Huang,* and Tushar Debnath**

Abstract: Mn-doping in cesium lead halide perovskite nanoplatelets (NPls) is of particular importance where strong quantum confinement plays a significant role towards the exciton–dopant coupling. In this work, we report an immiscible bi-phasic strategy for post-synthetic Mn-doping of $CsPbX_3$ (X = Br, Cl) NPls. A systematic study shows that electron-donating oleylamine acts as a shuttle ligand to transport MnX_2 through the water–hexane interface and deliver it to the NPls. The halide anion also plays an essential role in maintaining an appropriate radius of Mn^{2+} and thus fulfilling the octahedral factor required for the formation of perovskite crystals. By varying the thickness of parent NPls, we can tune the dopant incorporation and, consequently, the exciton-to-dopant energy transfer process in doped NPls. Time-resolved optical measurements offer a detailed insight into the exciton-to-dopant energy transfer process. This new approach for post-synthetic cation doping paves a way towards exploring the cation exchange process in several other halide perovskites at the polar–nonpolar interface.

Introduction

The introduction of dopants into colloidal semiconductor nanocrystals (NCs) can lead to outstanding optical, electrical and magnetic properties because of the strong exchange interaction between the excitons of host NCs and the dopant ions.[1] In particular, Mn^{2+} ion doping in several semiconductor NCs has been reported to introduce exciton-to-dopant energy transfer and charge transfer, responsible for improved performance of light-emitting diodes (LED) and solar cells, respectively.[2] In the past few years, Mn-doping has been used to improve the chemicophysical properties of cesium lead-halide perovskite NCs ($CsPbX_3$ PNCs, X = halide ion).[3] Extensive efforts have been devoted to developing different synthetic strategies for Mn-doped PNCs of various compositions and morphologies to tailor their optical properties.[4] Most of these methods for doping simply employ direct synthetic routes where all the perovskite precursors and the dopant element are added in one pot. However, the perovskite precursors tend to grow into PNCs without the dopant element due to bond-energy mismatch between Pb–X and Mn–X bond where $E_{Pb-X} < E_{Mn-X}$, making such doping processes less efficient.[3a,d] Increasing the reaction temperature and prolonging the reaction time are effective ways to achieve Mn-doped PNCs.[3c] However, overcoming the bond-energy mismatch through high temperature and long reaction time may compromise the control of morphology and size of the product.

In contrast, the chemical transformation approach (e.g. from Cs_4PbX_6 to $CsPbX_3$), also known as the post-synthetic method, has proven versatile not only to vary the phase structures but also to tailor the morphology of the pre-synthesized host PNCs.[5] The doping process has also been achieved by taking advantage of the phase structure transformation via a post-synthetic approach.[5a,6] The latter provides an effective way for tuning the photoluminescence (PL) of PNCs across the entire visible region via the halide anion exchange reaction.[7] The post-synthetic cation doping (e.g. Mn^{2+}-ion), however, is often limited to a single phase and for the limited reported bi-phasic strategy it requires the

[*] L. Wu,[+] Dr. Y. Wang,[+] M. Kurashvili, Dr. A. Dey, Prof. Dr. J. Feldmann, Prof. Dr. H. Huang, Dr. T. Debnath
Chair for Photonics and Optoelectronics, Nano-Institute Munich
Department of Physics, Ludwig-Maximilians-Universität München
Königinstr. 10, 80539 München (Germany)
E-mail: t.debnath@physik.uni-muenchen.de

L. Wu,[+] Dr. M. Cao, Prof. Dr. Q. Zhang
Institute of Functional Nano and Soft Materials (FUNSOM) Jiangsu Key Laboratory for Carbon-Based Functional Materials and Devices, Soochow University
199 Ren'ai Road, Suzhou 215123, Jiangsu (P. R. China)
E-mail: qiaozhang@suda.edu.cn

Dr. M. Döblinger
Department of Chemistry, Ludwig-Maximilians-Universität München, Butenandtstrasse 5–13 (E), 81377 München (Germany)

Prof. Dr. H. Huang
School of Optoelectronic Science and Engineering & Collaborative Innovation Center of Suzhou Nano Science and Technology
Soochow University, Suzhou 215006 (P. R. China)
E-mail: hh@suda.edu.cn

[+] These authors contributed equally to this work.

presence of a miscible polar solvent (DMF, acetone or acid such as HBr), which cannot be separated from the phase containing doped-PNCs and, therefore, sacrifices the quality and stability of the product.[6] In this regard, a recent report by Nag et al. has established a precipitation approach for separating the Mn-doped $CsPbX_3$ PNCs and nanoplatelets (NPls) from a mixed acetone–toluene (1:3 v/v) solvent and redispersing them in hexane in order to maintain the stability.[6b] However, the presence of acetone during the doping may partially destroy the NPls and thereby affects the long-term stability. Additionally, the relatively low solubility of Mn-precursor ($MnBr_2$ in this case) in the acetone–toluene mixture limits the amount of doping into the perovskite lattice.

Herein, we report an immiscible bi-phasic strategy for the post-synthetic Mn-doping in $CsPbX_3$ NPls (where X = Br, Cl) via the water–hexane interface and propose the possible mechanism of the one-step post-synthetic (OPS) doping. In such a two-phase system, the polar solvent water allows for a large amount of dissolved MnX_2 salt (up to 146 g/100 mL at 20 °C) for doping and is intrinsically separated from the hexane phase containing NPIs, which helps to maintain the quality and stability of the product. The electron-donating ligand oleylamine (OLA) acts as a molecular shuttle at the water–hexane interface to transport MnX_2 from water to hexane. The successful doping into the NPls can be corroborated by the presence of the characteristic Mn-related broad PL at ≈620 nm due to an exciton-to-dopant energy transfer. Moreover, time-resolved optical measurements provide fundamental insights into the doping as well as the energy transfer mechanism.

Results and Discussion

The schematic illustration of OLA-assisted post-synthetic MnX_2 doping in perovskite NPls via the polar–nonpolar interface is illustrated in Figure 1a. First, $CsPbBr_3$ NPls were prepared according to a procedure reported previously, containing both OLA and oleic acid (OA) as surface-passivating ligands.[8] The NPls dispersed in hexane show blue PL under UV-light irradiation (Figure 1a, left, inset). Different amounts of MnX_2 were dissolved in water to achieve a range of precursor concentrations. Then the MnX_2 aqueous solution was added into the hexane solution of the NPls in a volume ratio of 1:40 (water:hexane) at room temperature and the resulting solution was stirred for 1 h. The upper phase contained Mn-doped NPls in hexane, while excess MnX_2 in water remained in the lower phase. By simply separating the upper phase containing Mn-doped $CsPbBr_3$ NPIs from the water phase, the obtained NPIs could remain in a more favorable environment compared to those fabricated in the presence of an inseparable polar solvent during and after doping.[6] The as-prepared Mn-doped NPls dispersed in hexane show intense pinkish PL under UV-light irradiation (Figure 1a, right, inset and Supporting Information Video 1).

The interface between water and hexane acts as a semi-permeable membrane. It allows for the transportation of Mn-dopant but separates NPls from the aqueous phase. Such an immiscible two-phase OPS method provides a clean environment for doping and helps improve the stability of doped NPls. Notably, the doping process requires a halide anion and the presence of the OLA ligand. The detailed mechanism of the post-synthetic two-phase doping process is demonstrated later.

To understand the morphology of the product before and after doping, electron diffraction and scanning transmission electron microscopy in high-angle annular dark-field (STEM-HAADF) mode was performed. For all samples, electron diffraction patterns show reflections consistent with single-phase orthorhombic $CsPbBr_3$ in [001] orientation along the beam direction (Figure S1).[9] Corresponding high-resolution STEM-HAADF images are in good agreement with this finding. Figure 1b and c show STEM-HAADF images of the 5-monolayer (ML) undoped $CsPbBr_3$ NPls obtained at a reaction temperature of 180 °C (hereafter Un-180 NPls). The particle size of Un-180 NPls determined by STEM-HAADF is 39 ± 9 nm × 13 ± 3 nm. By controlling the concentration of $MnBr_2$ in the aqueous solution (2 M, 4 M and a saturated ≈7 M in the present study), one can achieve different amounts of Mn^{2+} doping into the NPls. Clearly, the morphology and shape of doped NPls remain unaltered even in the presence of a saturated $MnBr_2$ aqueous solution (≈7 M, noted as Mn-180 (7 M)) (Figure 1d). The lateral dimension of these NPls is 37 ± 8 nm × 12 ± 3 nm. Figure 1e shows a STEM-HAADF image of Mn-180 (4 M) NPls, revealing the absence of Ruddlesden–Popper (RP) type defects as observed previously for Mn-doped $CsPbCl_3$ NCs.[10] The unaffected crystallinity after doping implied that the physical structure is not the reason for the observed PL color change from blue to pinkish. Additional STEM-HAADF images are also available in Figure S2. In the present work, we have not observed any RP defects in the doped NPls samples, even with the highest concentration of Mn^{2+}. There are two possible reasons: first, in the previous work, the doped NCs were synthesized via a one-pot ultrasonication approach, while the present work conducted soft bi-phasic post-synthetic doping. Second, the cubic NCs employed in the previous work may be more susceptible to forming such defects within a single crystal than in the thin NPls employed in this work.

To confirm the success of Mn-doping, we performed Inductively Coupled Plasma-Optical Emission-Spectrometry (ICP-OES) and Electron Paramagnetic Resonance (EPR) measurements. While the former measurement allows us to determine the atomic percentage of Mn-doping in the host NPls, the latter measurement not only allows us to confirm the presence of Mn-dopant within the host but also gives valuable insights into their location in the crystal. Table S1 summarizes the measured Mn and Pb amounts via ICP-OES measurement in the 4 M and 7 M Mn-doped $CsPbBr_3$ NPls, which shows ≈4.2 % doping for 4 M and ≈8 % doping for 7 M Mn-doped NPls. Figure 2f shows the room-temperature EPR spectra of low (2 M) and high (7 M) Mn-doped $CsPbBr_3$ NPls. The EPR spectrum of the undoped sample shows no extra feature than the baseline of the empty tube (Figure S3). In the

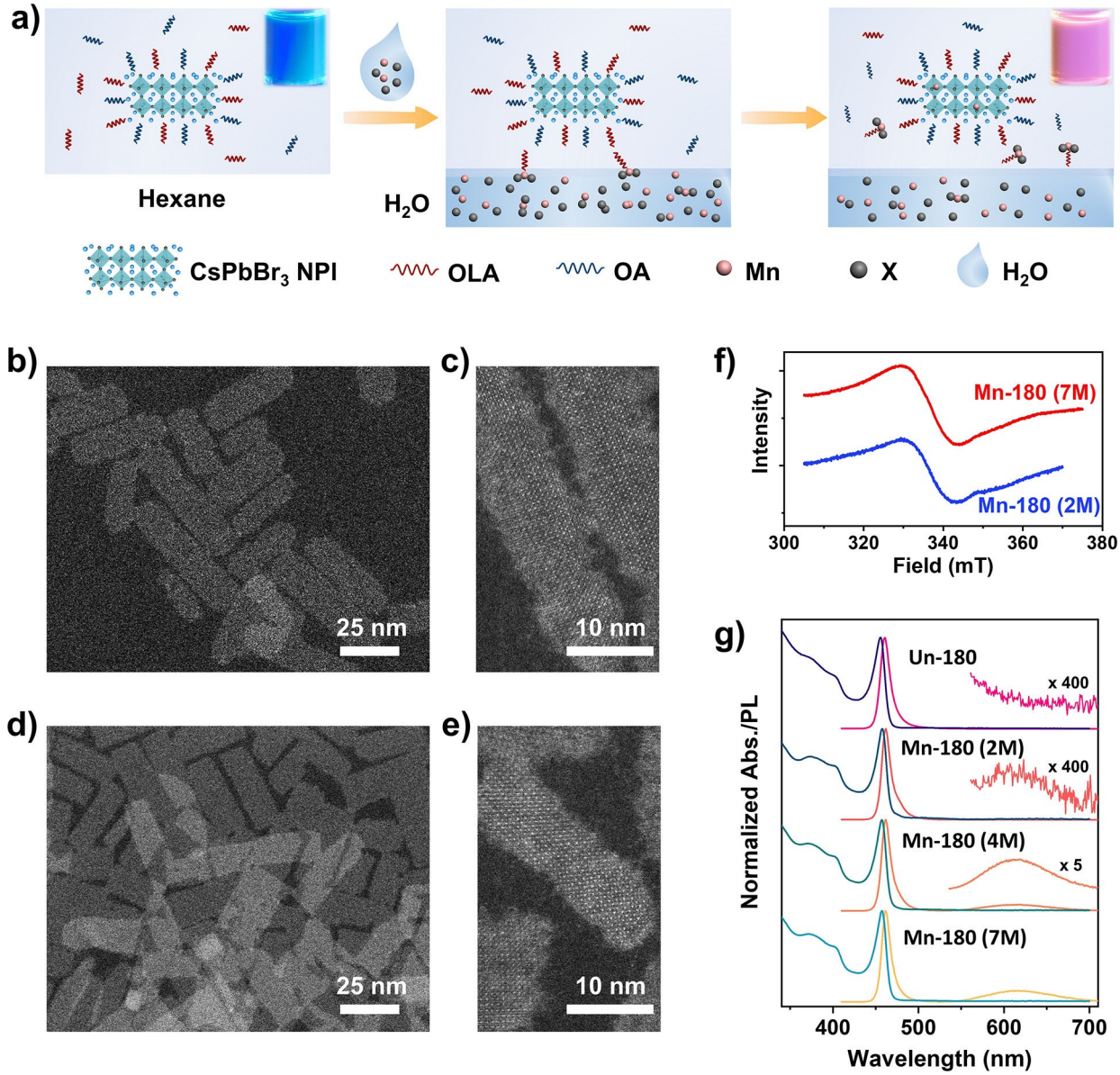

Figure 1. One-step post-synthetic (OPS) Mn-doping in $CsPbBr_3$ NPls. a) Schematic illustration of one-step post-synthetic Mn-doping in $CsPbBr_3$ NPls at the water–hexane interface, triggered by OLA as a shuttle ligand for the transport of MnX_2. The inset shows the PL under the UV-light irradiation of the undoped (left, blue) and Mn-doped (right, pinkish) $CsPbBr_3$ NPls. STEM-HAADF images of b), c) Un-180, d) Mn-180 (7 M) and e) Mn-180 (4 M) $CsPbBr_3$ NPls. f) EPR spectra of Mn-180 (2 M) and Mn-180 (7 M) $CsPbBr_3$ NPls at room temperature. g) UV/Vis absorption and PL spectra of Un-180 and Mn-180 $CsPbBr_3$ NPls with various concentrations of $MnBr_2$ in water. The inset shows the expanded view of the PL in the region 550–710 nm for Un-180 and Mn-180 (2 M and 4 M) $CsPbBr_3$ NPls.

NPls with both low and higher amounts of Mn-dopant the expected six individual lines collapse into one broad spectrum. Similar observation was made earlier with both low and high dopant amounts, which was ascribed to the enhancement of the antiferromagnetic coupling between Mn ions in the bulk of the NCs.[11] We further determined the hyperfine coupling constant (A) to be ≈12 mT, higher than the previous report.[11a] Therefore, we believe in the present case, the dopants are located in the bulk of the NPls, giving rise to a strong Mn–Mn antiferromagnetic interaction, resulting in the observed large A-value. A further detailed study to quantify the effect of Mn–Mn interaction is under investigation.

To investigate the optical properties of the doped NPls, we performed UV/Vis absorption and PL measurements on the undoped and Mn-doped NPls (Figure 1g). The Un-180 NPls show a sharp and strong excitonic resonance at ≈456 nm in the absorption spectrum due to its large exciton binding energy (100's of meV).[12] The corresponding PL spectrum shows a single, sharp peak at ≈461 nm, corresponding to a 5 monolayer (ML) sample.[8] Though the absorption spectra remain almost unchanged upon Mn^{2+} doping, an additional broad PL appears in the region of

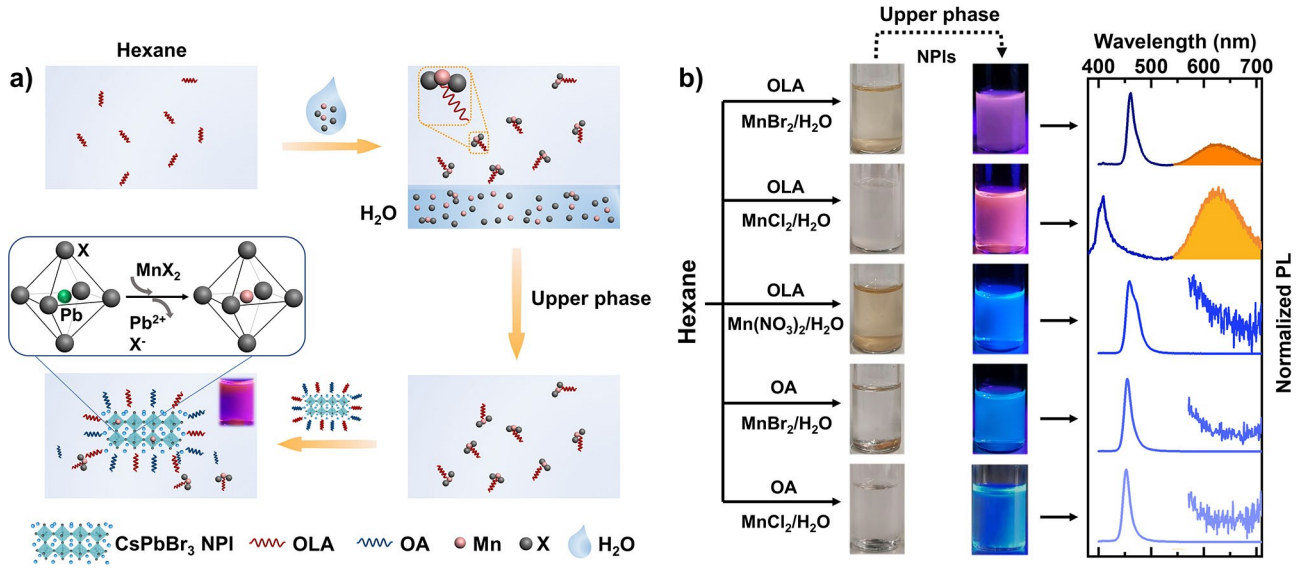

Figure 2. The functions of halide ions and ligands in Mn-doping in $CsPbBr_3$ NPls. a) Schematic of the bi-phasic two-step post-synthetic (TPS) Mn-doping in $CsPbBr_3$ NPls, revealing the shuttle role of the OLA at the water–hexane interface, responsible for the MnX_2 transport. The inset in the middle shows the mechanism of MnX_2 doping at the lead–halide octahedral. b) The two-step synthesis of the post-synthetic Mn-doping in $CsPbBr_3$ NPls: in the first step, different precursor solutions containing appropriate dopants and ligands in the respective phases are shown in ambient lighting. In the second step, the upper phase from the first step is added into the $CsPbBr_3$ NPls solutions. Their images are shown under UV illumination. The rightmost panel compares the corresponding PL spectra (the inset shows the 400 times expanded view of the PL in the region 550–710 nm for the last three cases). During the first step, an aqueous solution of saturated Mn-precursor is used for all the cases.

550–700 nm, with a maximum at ≈618 nm, along with the excitonic PL at ≈461 nm. The new broad PL at ≈618 nm can be attributed to the Mn^{2+}-related d–d transition (the $^4T_1$–$^6A_1$ transition), implying the successful doping of Mn^{2+} into the $CsPbBr_3$ NPls.[3c,4b] The excitonic absorption and PL position are not affected by the amount of Mn-doping (Figure 1g). In contrast, the PL intensity due to Mn^{2+}-related d–d transition increases drastically with increased $MnBr_2$ concentration in water, indicating an enhancement in the incorporation of dopant (Figure 1g). Furthermore, the PL quantum yield (PLQY) of the undoped NPls (Un-180) was measured to be only ≈6 %, which resembles our earlier work.[12] However, the PLQY enhances significantly upon Mn-doping, i.e. to ≈17 % and ≈23 % for the 4 M and 7 M Mn-180 NPls, respectively. One should note that the PL under UV illumination does not show a typical orange color, but appears pinkish (Figure 1a) even for the highest Mn-doping concentration (≈7 M). Here the PL of the Mn-doped NPls under the UV illumination results from the intense blue exciton PL and a weak orange Mn-PL. The above results clearly confirm that this OPS approach can successfully dope Mn^{2+} into the NPls.

Then the mechanism involved in this method was studied carefully. To this end, we developed a two-step post-synthesis (TPS) approach to reveal the roles of halide ions and ligands (OLA and OA) individually. Note that this TPS approach is different from the above-described OPS method, where only a single step is involved during the post-synthesis process. In an ideal two-step approach (Figure 2a), the first step is to acquire Mn^{2+} precursor from the aqueous solution to the hexane containing only one type of ligand (OLA or OA). The second step is to add the Mn^{2+}-enriched hexane to NPls to perform the doping. We first added a saturated aqueous solution of a Mn-salt (MnX_2 or $Mn(NO_3)_2$) into hexane containing either OLA or OA and then stirred the mixture for about 1 min. Then the upper phase that primarily contains ligands in hexane was separated and added to the undoped $CsPbBr_3$ NPls dispersed in hexane (Supporting Information Video 2). Figure 2b compares the corresponding PL under the UV illumination along with the PL spectra for different precursor solutions (an individual Mn-salt as well as a ligand of OLA or OA). From the PL spectra, one can clearly see that when OLA was used as the only ligand, Mn^{2+} could be doped into the $CsPbBr_3$ or $CsPb(Cl/Br)_3$ NPls, using either $MnBr_2$ or $MnCl_2$ as a precursor, respectively. The corresponding PL spectra reveal the characteristic Mn^{2+} emission at ≈624 nm, along with the exciton PL at 461 and 409 nm, respectively. The PL spectrum of the Mn-doped $CsPb(Cl/Br)_3$ NPls unveils an intense Mn^{2+} emission due to an efficient exciton-to-dopant energy transfer phenomenon, typical for such Cl-based NPls, compared to the pure bromide case.[4b] Previously, Cui et al. reported the doping of Mn^{2+} into $CsPbBr_3$ NCs, which only works using $MnCl_2$ as the precursor (thus limited to a mixed halide perovskite NCs), unlike the present work, albeit the reaction was performed in the DMF/hexane mixture.[6a]

When $Mn(NO_3)_2$ was used as a precursor in the TPS method, the upper phase turned brownish after stirring (Figure 2b), indicating that Mn^{2+} was transferred to hexane in the presence of OLA. However, when the upper

phase containing Mn^{2+} was added to NPIs, the doping was unsuccessful, as evidenced by the absence of the Mn^{2+} peak in the PL spectrum (Figure 2b, $Mn(NO_3)_2$). In other words, Mn^{2+} (from Mn $(NO_3)_2$) could be transported into hexane but could not achieve the further doping. In order to validate the phenomenon, we also performed the OPS strategy using $MnCl_2$ or $Mn(NO_3)_2$ as the precursor in water (as described in the context of Figure 1). Again, while $MnCl_2$ could achieve the doping, $Mn(NO_3)_2$ failed to dope Mn^{2+} into the NPls (Figure S4), suggesting the unique functions of the halide anions. These anions might enter the hexane from water as ligands in the coordination with Mn^{2+} and OLA, as evidenced by the blue-shifted exciton PL signal due to the halide exchange between Br and Cl with $MnCl_2$ as the precursor (Figure 2b, $MnCl_2$). One distinct difference is that halide anions are stronger electron donors compared to nitrate anions, which are electron acceptors. The different electronic properties of both anion ligands result in the difference in energy between the d orbitals (Δ) in forming an octahedral complex. In the presence of Br^-, Cl^- anions, Mn^{2+} forms a high-spin state with an effective ionic radius of around 83 pm.[13] In contrast, the effective ionic radius of Mn^{2+} at a low-spin state is reduced to 67 pm in the presence of NO_3^-.[13] Such a decrease in radius corresponds to a drop in the octahedral factor ($\mu = r_{Mn^{2+}}/r_{Br^-}$) of the potential crystal unit containing Mn^{2+} and Br^- (radius of 196 pm) from 0.423 to 0.342,[13] falling out of the range of possible radius ratio (0.41–0.9).[14] In this case, Mn^{2+} from Mn-$(NO_3)_2$ cannot sufficiently stabilize the crystal structure and hence is unlikely to replace Pb^{2+} in the $CsPbBr_3$ NPIs. This result provides an important insight for a post-synthetic doping mechanism that the halide anion plays an essential role in maintaining an appropriate radius of Mn^{2+} and thereby the octahedral factor required for the crystal formation.

The role of ligands in the doping process was then investigated systematically. In the colloidal dispersion of NPls in hexane, some excess ligands are always available, which are in equilibrium between adsorption and desorption on the NPls surface.[15] It is possible that some of the ligands, such as OLA, may escape from the NPls surface towards the water–hexane interface and act as a shuttle ligand to transport MnX_2 from the aqueous phase to hexane. With the assistance of excess ligands available at the interface, MnX_2 may be brought into the hexane and reach the NPls to achieve the doping. In the OPS method, we propose that the amount of Mn^{2+} delivered to the NPls from the aqueous phase could depend on the total amount of MnX_2 present in the interface and the available shuttle ligands in the upper phase. Similarly, in this TPS strategy, OLA could act as a molecular shuttle to transport MnX_2 at the water–hexane interface. This may result in the brownish color on the upper phase in the first step (the top two cases in Figure 2b) and, subsequently, the appearance of PL due to the Mn^{2+} related d–d transition in the second step. In contrast, when only OA was used as a ligand while the other parameters were kept the same, no color change could be observed in the upper phase, indicating the absence of Mn^{2+} ions (the bottom two cases in Figure 2b), which has been further confirmed by the missing characteristic PL of the Mn^{2+} d–d transition. This observation further proved the critical shuttling role of OLA ligands.

Unlike OA containing a weak electron acceptor of carboxyl group, the amine group in OLA is a strong electron donor, favorable for coordination with Mn^{2+}. Such coordination assists the transportation from the aqueous phase to hexane, which is consistent with a previous study, showing the kinetics of the Pb-oleate formation is slower than the kinetically favorable coordination of OLA to Pb^{2+}.[16] If the hexane contains no ligands in the first step, the doping was unsuccessful even when a saturated MnX_2 aqueous solution was used (Figure S5). With a higher OLA amount, not only does the incorporation of Mn^{2+} increase in $CsPbBr_3$ NPls (as evidenced by the stronger Mn PL intensity) but also the incorporation of Cl^- was enhanced, as can be seen from the blue-shift of the exciton peak (Figure S6). This result further indicates the critical shuttling function of the OLA during the MnX_2 doping. Therefore, it is proposed that OLA acts as a shuttle ligand for the MnX_2 transport at the water–hexane interface and delivers the MnX_2 directly to the NPls in hexane. In short, the bi-phasic post-synthetic doping (both OPS and TPS) method developed in this work not only requires the presence of halide ions but is also triggered by the shuttling behavior of the OLA at the water–hexane interface, leading to the MnX_2 doping.

Though the newly developed OPS approach can successfully dope Mn^{2+} into the $CsPbBr_3$ NPls, the amount of dopant incorporated is small, resulting in a weak exciton-to-dopant energy transfer that can be rationalized from the observed weak PL due to the Mn^{2+} d–d transition. To further increase the amount of dopant incorporation, we prepared undoped $CsPbBr_3$ NPls with various thicknesses at different reaction temperatures, (100, 150 and 180 °C). Figure 3a and b represent the corresponding absorption and PL spectra of the undoped and Mn-doped (7 M) $CsPbBr_3$ NPls, respectively. The corresponding STEM-HAADF images are shown in Figure 1b, d and Figure 3c–f. Figure S7–S9 summarizes the additional optical absorption and PL spectra for the undoped (different thickness) and doped NPls as a function of different reaction times as well as several $MnBr_2$-precursor concentrations. Interestingly, we observed an enhancement in the Mn^{2+} PL intensity in the doped NPls for the parent NPls with a smaller thickness (i.e. Mn-100 > Mn-150 > Mn-180), due to an enhanced exciton-to-dopant energy transfer process (Figure 3b). The above result provides direct insight that by varying the thickness of the parent NPls, one can tune the Mn incorporation easily. One should note, the Mn PL peak position, which appears at $\approx$618 nm for the Mn-180 (7 M) NPls, blue-shifted upon reduction of the parent NPls thickness; for example, the Mn PL appears at $\approx$608 nm and $\approx$605 nm for Mn-150 (7 M) and Mn-100 (7 M) NPls, respectively. The blue-shift in Mn PL arises possibly due to the enhanced ligand field interaction of Mn^{2+} ions with the surrounding ligands, leading to more splitting of the Mn^{2+} $^4T_1$–$^6A_1$ energy (see Supporting Information section 3.1 and 3.2).[17] Moreover, we performed a detailed investigation of the stability of undoped and

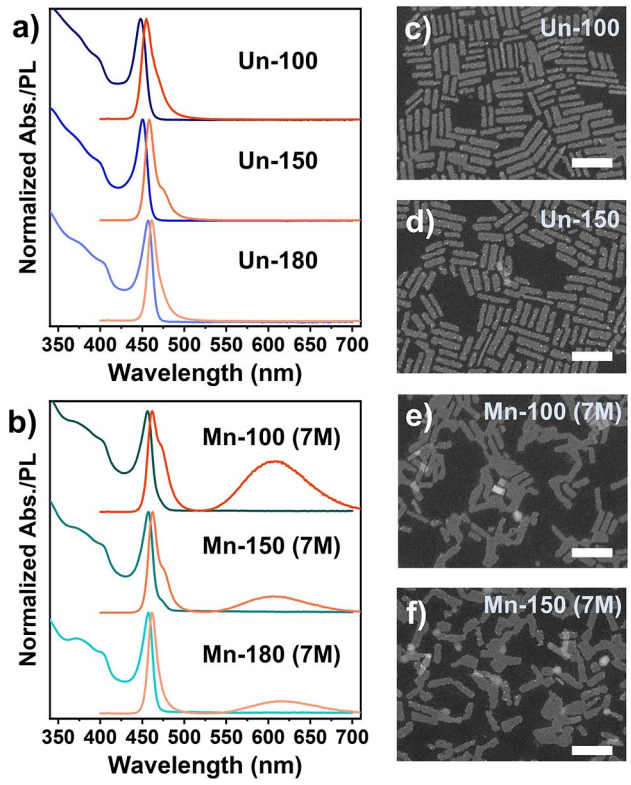

Figure 3. The Mn-doping in $CsPbBr_3$ NPls with different thicknesses. UV/Vis absorption and PL spectra of a) undoped and b) Mn-doped (7 M) $CsPbBr_3$ NPls, with the parent NPls obtained at various reaction temperatures between 100 and 180 °C to tailor the thickness. c)–f) STEM-HAADF images of undoped and Mn-doped $CsPbBr_3$ NPls, with the parent NPls obtained at 100 and 150 °C, respectively. All scale bars are 50 nm. An aqueous solution of saturated $MnBr_2$ (≈7 M) is used for all the cases.

doped NPls prepared at 100 and 180 °C at ambient condition, by probing the PL spectra. As shown in Figure S10–S12, the NPls prepared at 100 °C is only stable for a few days (<10 days), while the one prepared at 180 °C is stable for more than 10 days, as the PL spectra remain unchanged on the 10th day, for both undoped and Mn-doped NPls. This indicates ambient humidity does not significantly affect perovskite stability if separated from the aqueous environment after stirring for 1 h. However, prolonged mixing (in days) of an aqueous solution with the NPls can degrade the perovskites, even if they were stored in a nitrogen atmosphere (Figure S12). A possible mechanism for how Mn-incorporation into the NPls can be controlled by the NPls thickness has been provided in the Supporting Information (Section 3.1), based on the stability of the undoped and the doped NPls prepared at 100 and 180 °C (Figure S10–S12).

To gain further insight into the exciton-to-dopant energy transfer in the prepared Mn-doped NPls, time-resolved PL measurements were performed. To this end, we probed the excitonic PL after excitation with a 365 nm laser for both undoped and a series of Mn-doped NPls prepared with various concentrations of Mn-precursor in water (Figure 4a). The PL decay of the Un-100 NPls can be fitted biexponen-

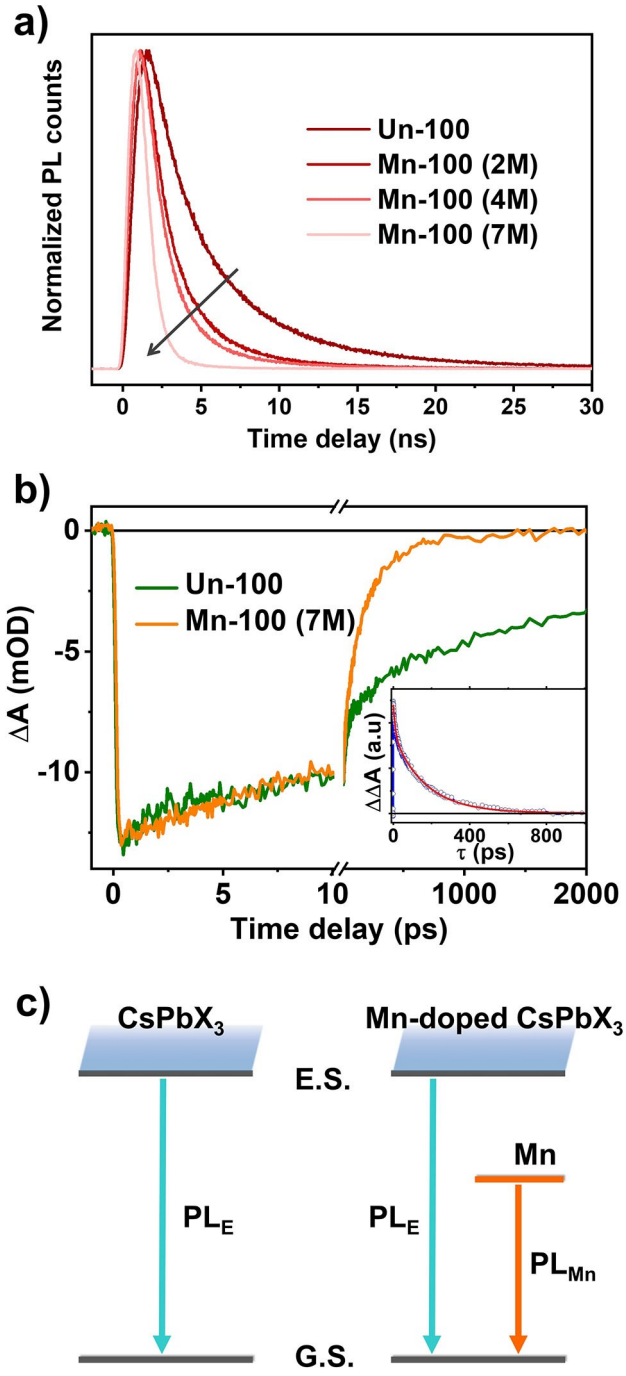

Figure 4. a) Time-resolved PL decay traces (λ_{ex} = 365 nm) of undoped and Mn-doped $CsPbBr_3$ NPls (with various concentrations of $MnBr_2$ in water) at the exciton position obtained at 100 °C during the parent NPl synthesis. b) Comparison of transient traces at the bleaching maxima of the undoped and 7 M Mn-doped $CsPbBr_3$ NPls obtained at 100 °C. Note the break in the time axis between 10 and 10.1 ps. Inset: The difference between the two transients ($\Delta\Delta A$) in (b), after normalizing at a longer time (≈ns). The solid red line in the inset represents the exponential fit. c) Schematic within the excitonic picture showing exciton PL in the undoped $CsPbX_3$ NPls. The Mn-doped $CsPbX_3$ NPls exhibit both exciton (PL_E) as well as Mn-related PL (PL_{Mn}), due to the excitonic energy transfer to the Mn-dopant, leading to a faster exciton PL decay compared to the undoped NPls. G.S. and E.S. represent ground and excited states, respectively.

tially with a fast 2.9 ns (76 %) and a slow 7.6 ns (24 %) component (having an average lifetime of 4 ns, Table S1). This result agrees with the previous report on a similar material which suggests that the radiative recombination is primarily due to the exciton rather than free charge carrier recombination.[4b,18] Interestingly, upon Mn-doping, the lifetime of both components decreases. Moreover, with increased Mn-concentration, the contribution of fast PL grows drastically and becomes the single exponential for Mn-100 (7 M) NPls with a lifetime of 0.8 ns (Table S1). Thus, we observe a reduction of the average exciton lifetime by a factor of 5 (4 ns vs. 0.8 ns) from Un-100 to Mn-100 (7 M) samples. Therefore, the faster exciton recombination observed upon doping should correspond to the exciton-to-dopant energy transfer process (see later). The results of the time-resolved PL experiments performed on the NPls prepared at 180 °C are shown in Figure S13. Similar to the observations made for Mn-100 samples, increasing Mn-concentration in Mn-180 samples reduces the exciton lifetime (Table S2), indicating an enhancement of the exciton-to-dopant energy transfer process. Notably, the average lifetime of excitons in the Mn-180 (7 M) NPls is reduced by a factor of 2.8 (3.1 ns vs. 1.1 ns) compared to the Un-180 NPls. As this reduction factor is directly related to the exciton-to-dopant energy transfer process, one may conclude that the energy transfer process is more efficient in the doped-NPls prepared at 100 °C (reduction factor 5) than those prepared at 180 °C (reduction factor 2.8). This also agrees with our previous discussion based on the PL measurements.

We also performed femtosecond transient absorption (TA) measurements and observed strong exciton bleaching for both undoped and Mn-doped NPls (Figure S14) due to phase-space-filling of the states contributing to the exciton state.[12,19] The corresponding transient time traces at the bleaching maxima for the undoped and 7 M Mn-doped NPls are shown in Figure 4b. Please note, as the 100 °C sample demonstrates the maximum energy transfer, it has been chosen as the representative sample in Figure 4b. The corresponding transient time traces of 180 °C samples are shown in Figure S15. While the early time (≈few ps) bleach recovery dynamics look identical for both the NPls, the recombination dynamics are much faster at the longer time delay (≈ns) for the Mn-doped NPls than the undoped NPls (Figure 4b and Figure S15), consistent with the time-resolved PL measurement. A similar result was reported for the undoped and Mn-doped CdSe as well as $CsPbCl_3$ NCs.[11a,20] Compared to the undoped NPls, the Mn-doped NPls has one additional de-activation channel of the exciton: the energy transfer from the exciton to the dopant ion (Figure 4c). Thus, the faster exciton recombination observed upon doping must correspond to the exciton-to-dopant energy transfer process. Therefore, by subtracting the two transients at the bleaching wavelength (after normalizing at a longer time delay ≈ns), we estimated the exciton-to-dopant energy transfer time for Mn-100 (7 M) and Mn-180 (7 M) NPls to be ≈168 ps and ≈311 ps, respectively (inset in Figure 4b, Figure S15 and Supporting Information section 3.3). The energy transfer efficiency (η) between the NPls exciton and the Mn-dopant, however, can be estimated using the following Equation (1):[21]

$$\eta = 1 - \frac{\gamma_{U_n}}{\gamma_{\mathrm{Mn}}} \quad (1)$$

where, γ_{U_n} and γ_{Mn} correspond to the rate of the bleach recovery process at longer time delay for undoped and Mn-doped NPls, respectively. Thus, the energy transfer efficiency of the Mn-180 (7 M) and Mn-100 (7 M) NPls was estimated to be ≈73 % and ≈91 %, respectively.

This observation is in sharp contrast to the Mn-doped II–VI based quantum dots, where significantly faster exciton-to-dopant energy transfer process was observed, in the orders of a few ps.[20b,22] Klimov et al. attributed such ultrafast exciton-to-dopant energy transfer process to an *sp–d* exchange type interaction between the quantum dot exciton and the Mn^{2+} ion,[22] suggesting that a Dexter type energy transfer mechanism is viable in such a system. In the present case, however, an at least two orders of magnitude slower energy transfer process is observed (100's of ps), similar to earlier reports in other perovskites,[20c] indicating a different type of energy transfer mechanism is active between the exciton and the Mn^{2+} ion in perovskite NPls (Figure 4c), possibly Förster type dipole–dipole interaction.

Conclusion

In summary, we have developed a strategy for bi-phasic post-synthetic Mn-doping (both OPS and TPS) into $CsPbX_3$ NPls at the polar–nonpolar interface with enhanced stability as a result of the easy separation of water from hexane. Utilizing the advantage of the high solubility of MnX_2 in water, we successfully doped a wide range of amounts of MnX_2 into the pre-synthesized NPls. The halide anion helps maintaining an appropriate radius of Mn^{2+}, consequently the octahedral factor for the perovskite crystal structure. Our detailed investigation reveals the shuttling role of the electron-donor OLA ligand at the water–hexane interface, which transports MnX_2 from water to the NPls in hexane. By varying the thickness of the parent NPls, we can tune the incorporation of Mn^{2+} further during the post-synthetic doping. Furthermore, we performed time-resolved PL and TA measurements to provide additional insights into the exciton-to-dopant energy transfer phenomenon. This directs that a slower Förster type dipole–dipole energy transfer may be active between perovskite and Mn-related transitions. This new strategy towards stable post-synthetic doping using the immiscible polar–nonpolar interface may be extended to other dopants in perovskite NCs.

Acknowledgements

We acknowledge financial support by the Bavarian State Ministry of Science, Research, and Arts through the grant

"Solar Technologies go Hybrid (SolTech)", the National Natural Science Foundation of China (51922073), the China Scholarship Council (L.W.), the Alexander von Humboldt Foundation (Y.W., A.D. and T.D.), the German–Israeli Foundation for Scientific Research and Development (GIF, Project I-1512-401.10/2019) (M.K.), the European Union's Horizon 2020 research and innovation program under the Marie Sklodowska-Curie grant agreement No. 839042 (H.H.). We thank local research clusters and centers such as the Center of Nanoscience (CeNS) and e-conversion for providing communicative networking structures. We also thank Sophie Gutenthaler and Rainer Götz for their assistance on ICP-OES and EPR measurements, respectively. We thank Shizhe Wang for the assistance on the schematic drawing. Open Access funding enabled and organized by Projekt DEAL.

Conflict of Interest

The authors declare no conflict of interest.

Data Availability Statement

The data that support the findings of this study are available from the corresponding author upon reasonable request.

Keywords: $CsPbX_3$ Nanoplatelets · Energy Transfer · Mn Doping · Shuttle Ligands · Water–Hexane Interface

[1] a) D. J. Norris, A. L. Efros, S. C. Erwin, *Science* **2008**, *319*, 1776–1779; b) N. Pradhan, D. Goorskey, J. Thessing, X. G. Peng, *J. Am. Chem. Soc.* **2005**, *127*, 17586–17587; c) R. Beaulac, P. I. Archer, S. T. Ochsenbein, D. R. Gamelin, *Adv. Funct. Mater.* **2008**, *18*, 3873–3891; d) B. B. Srivastava, S. Jana, N. Pradhan, *J. Am. Chem. Soc.* **2011**, *133*, 1007–1015.

[2] a) R. Beaulac, P. I. Archer, J. van Rijssel, A. Meijerink, D. R. Gamelin, *Nano Lett.* **2008**, *8*, 2949–2953; b) D. Mocatta, G. Cohen, J. Schattner, O. Millo, E. Rabani, U. Banin, *Science* **2011**, *332*, 77–81; c) N. Pradhan, D. D. Sarma, *J. Phys. Chem. Lett.* **2011**, *2*, 2818–2826; d) P. K. Santra, P. V. Kamat, *J. Am. Chem. Soc.* **2012**, *134*, 2508–2511; e) J. Wang, Y. Li, Q. Shen, T. Izuishi, Z. Pan, K. Zhao, X. Zhong, *J. Mater. Chem. A* **2016**, *4*, 877–886; f) T. Debnath, H. N. Ghosh, *J. Phys. Chem. C* **2019**, *123*, 10703–10719; g) V. Pinchetti, A. Anand, Q. A. Akkerman, D. Sciacca, M. Lorenzon, F. Meinardi, M. Fanciulli, L. Manna, S. Brovelli, *ACS Energy Lett.* **2019**, *4*, 85–93; h) P. K. R., R. Viswanatha, *APL Mater.* **2020**, *8*, 020901.

[3] a) W. Y. Liu, Q. L. Lin, H. B. Li, K. F. Wu, I. Robel, J. M. Pietryga, V. I. Klimov, *J. Am. Chem. Soc.* **2016**, *138*, 14954–14961; b) D. Parobek, B. J. Roman, Y. T. Dong, H. Jin, E. Lee, M. Sheldon, D. H. Son, *Nano Lett.* **2016**, *16*, 7376–7380; c) A. K. Guria, S. K. Dutta, S. Das Adhikari, N. Pradhan, *ACS Energy Lett.* **2017**, *2*, 1014–1021; d) H. Liu, Z. Wu, J. Shao, D. Yao, H. Gao, Y. Liu, W. Yu, H. Zhang, B. Yang, *ACS Nano* **2017**, *11*, 2239–2247; e) X. Yuan, S. Ji, M. C. De Siena, L. Fei, Z. Zhao, Y. Wang, H. Li, J. Zhao, D. R. Gamelin, *Chem. Mater.* **2017**, *29*, 8003–8011.

[4] a) Q. A. Akkerman, D. Meggiolaro, Z. Y. Dang, F. De Angelis, L. Manna, *ACS Energy Lett.* **2017**, *2*, 2183–2186; b) W. J. Mir, M. Jagadeeswararao, S. Das, A. Nag, *ACS Energy Lett.* **2017**, *2*, 537–543.

[5] a) J. Ren, X. Zhou, Y. Wang, *Nano Res.* **2020**, *13*, 3387–3395; b) H. Hu, L. Wu, Y. Tan, Q. Zhong, M. Chen, Y. Qiu, D. Yang, B. Sun, Q. Zhang, Y. Yin, *J. Am. Chem. Soc.* **2018**, *140*, 406–412; c) L. Wu, H. Hu, Y. Xu, S. Jiang, M. Chen, Q. Zhong, D. Yang, Q. Liu, Y. Zhao, B. Sun, Q. Zhang, Y. Yin, *Nano Lett.* **2017**, *17*, 5799–5804; d) D. Yang, P. Li, Y. Zou, M. Cao, H. Hu, Q. Zhong, J. Hu, B. Sun, S. Duhm, Y. Xu, Q. Zhang, *Chem. Mater.* **2019**, *31*, 1575–1583.

[6] a) G. Huang, C. Wang, S. Xu, S. Zong, J. Lu, Z. Wang, C. Lu, Y. Cui, *Adv. Mater.* **2017**, *29*, 1700095; b) W. J. Mir, Y. Mahor, A. Lohar, M. Jagadeeswararao, S. Das, S. Mahamuni, A. Nag, *Chem. Mater.* **2018**, *30*, 8170–8178; c) W. J. Mir, A. Swarnkar, A. Nag, *Nanoscale* **2019**, *11*, 4278–4286.

[7] a) G. Nedelcu, L. Protesescu, S. Yakunin, M. I. Bodnarchuk, M. J. Grotevent, M. V. Kovalenko, *Nano Lett.* **2015**, *15*, 5635–5640; b) Q. A. Akkerman, V. D'Innocenzo, S. Accornero, A. Scarpellini, A. Petrozza, M. Prato, L. Manna, *J. Am. Chem. Soc.* **2015**, *137*, 10276–10281.

[8] D. Yang, Y. Zou, P. Li, Q. Liu, L. Wu, H. Hu, Y. Xu, B. Sun, Q. Zhang, S.-T. Lee, *Nano Energy* **2018**, *47*, 235–242.

[9] S. Hirotsu, J. Harada, M. Iizumi, K. Gesi, *J. Phys. Soc. Jpn.* **1974**, *37*, 1393–1398.

[10] S. Paul, E. Bladt, A. F. Richter, M. Doblinger, Y. Tong, H. Huang, A. Dey, S. Bals, T. Debnath, L. Polavarapu, J. Feldmann, *Angew. Chem. Int. Ed.* **2020**, *59*, 6794–6799; *Angew. Chem.* **2020**, *132*, 6860–6865.

[11] a) A. De, N. Mondal, A. Samanta, *Nanoscale* **2017**, *9*, 16722–16727; b) T. Qiao, X. Liu, D. Rossi, M. Khurana, Y. Lin, J. Wen, J. Cheon, A. V. Akimov, D. H. Son, *Nano Lett.* **2021**, *21*, 9543–9550.

[12] B. J. Bohn, Y. Tong, M. Gramlich, M. L. Lai, M. Döblinger, K. Wang, R. L. Z. Hoye, P. Müller-Buschbaum, S. D. Stranks, A. S. Urban, L. Polavarapu, J. Feldmann, *Nano Lett.* **2018**, *18*, 5231–5238.

[13] a) R. D. Shannon, *Acta Crystallogr. Sect. A* **1976**, *32*, 751–767; b) R. D. Shannon, C. T. Prewitt, *Acta Crystallogr. Sect. B* **1969**, *25*, 925–946; c) R. D. Shannon, C. T. Prewitt, *Acta Crystallogr. Sect. B* **1970**, *26*, 1046–1048.

[14] a) C. Li, X. Lu, W. Ding, L. Feng, Y. Gao, Z. Guo, *Acta Crystallogr. Sect. B* **2008**, *64*, 702–707; b) D. Ji, S. Feng, L. Wang, S. Wang, M. Na, H. Zhang, C. Zhang, X. Li, *Vacuum* **2019**, *164*, 186–193.

[15] a) M. Kazes, T. Udayabhaskararao, S. Dey, D. Oron, *Acc. Chem. Res.* **2021**, *54*, 1409–1418; b) R. Grisorio, M. E. Di Clemente, E. Fanizza, I. Allegretta, D. Altamura, M. Striccoli, R. Terzano, C. Giannini, M. Irimia-Vladu, G. P. Suranna, *Nanoscale* **2019**, *11*, 986–999; c) A. Dey, J. Ye, A. De, E. Debroye, S. K. Ha, E. Bladt, A. S. Kshirsagar, Z. Wang, J. Yin, Y. Wang, L. N. Quan, F. Yan, M. Gao, X. Li, J. Shamsi, T. Debnath, M. Cao, M. A. Scheel, S. Kumar, J. A. Steele, M. Gerhard, L. Chouhan, K. Xu, X.-g. Wu, Y. Li, Y. Zhang, A. Dutta, C. Han, I. Vincon, A. L. Rogach, A. Nag, A. Samanta, B. A. Korgel, C.-J. Shih, D. R. Gamelin, D. H. Son, H. Zeng, H. Zhong, H. Sun, H. V. Demir, I. G. Scheblykin, I. Mora-Seró, J. K. Stolarczyk, J. Z. Zhang, J. Feldmann, J. Hofkens, J. M. Luther, J. Pérez-Prieto, L. Li, L. Manna, M. I. Bodnarchuk, M. V. Kovalenko, M. B. J. Roeffaers, N. Pradhan, O. F. Mohammed, O. M. Bakr, P. Yang, P. Müller-Buschbaum, P. V. Kamat, Q. Bao, Q. Zhang, R. Krahne, R. E. Galian, S. D. Stranks, S. Bals, V. Biju, W. A. Tisdale, Y. Yan, R. L. Z. Hoye, L. Polavarapu, *ACS Nano* **2021**, *15*, 10775–10981.

[16] H. Huang, J. Raith, S. V. Kershaw, S. Kalytchuk, O. Tomanec, L. Jing, A. S. Susha, R. Zboril, A. L. Rogach, *Nat. Commun.* **2017**, *8*, 996.

[17] A. Hazarika, A. Layek, S. De, A. Nag, S. Debnath, P. Mahadevan, A. Chowdhury, D. D. Sarma, *Phys. Rev. Lett.* **2013**, *110*, 267401.
[18] L. Protesescu, S. Yakunin, M. I. Bodnarchuk, F. Krieg, R. Caputo, C. H. Hendon, R. X. Yang, A. Walsh, M. V. Kovalenko, *Nano Lett.* **2015**, *15*, 3692–3696.
[19] T. Debnath, D. Sarker, H. Huang, Z.-K. Han, A. Dey, L. Polavarapu, S. V. Levchenko, J. Feldmann, *Nat. Commun.* **2021**, *12*, 2629.
[20] a) T. Debnath, P. Maity, S. Maiti, H. N. Ghosh, *J. Phys. Chem. Lett.* **2014**, *5*, 2836–2842; b) H.-Y. Chen, S. Maiti, D. H. Son, *ACS Nano* **2012**, *6*, 583–591; c) D. Rossi, D. Parobek, Y. Dong, D. H. Son, *J. Phys. Chem. C* **2017**, *121*, 17143–17149.
[21] C. Blum, N. Zijlstra, A. Lagendijk, M. Wubs, A. P. Mosk, V. Subramaniam, W. L. Vos, *Phys. Rev. Lett.* **2012**, *109*, 203601.
[22] R. Singh, W. Liu, J. Lim, I. Robel, V. I. Klimov, *Nat. Nanotechnol.* **2019**, *14*, 1035–1041.

Manuscript received: November 21, 2021
Accepted manuscript online: January 7, 2022
Version of record online: February 3, 2022